12

Improvement in Corrosion Fatigue Resistance of Mg Alloy due to Plating

Sotomi Ishihara[1], Hisakimi Notoya[2] and Tomonori Namito[1]
[1]*Dept. Of Mechanical Engineering, University of Toyama*
[2]*Takamatsu Plating Co. Ltd.*
Japan

1. Introduction

Magnesium alloys are very attractive as structural materials, because they are extremely light, possessing excellent specific tensile strength, good stiffness, good cutting performance, and good vibrational absorption [1]. In addition, the recycling energy requirement of these alloys is only 4–5% of the energy required to obtain magnesium from the ore [1]. Due to their energy and weight saving characteristics, magnesium alloy are considered to be good candidates for material in auto parts, portable personal computers, and telephones.
However, magnesium alloys have not been extensively used until recently, because of their vulnerability to corrosion. When considering the use of magnesium alloys as structural materials, a thorough understanding of the corrosion-fatigue characteristics is necessary to reflect the results in machine design. Further, improvement in the corrosion fatigue performance of magnesium alloys is highly desirable to realize their potential as structural materials.
Surface treatments, such as coating or plating of the material surface have been examined for enhancement of the corrosion fatigue resistance of magnesium alloys, and in general they have not been successful.
In this paper, two types of plating treatments, i.e., electroless-Ni-plating [2] and electrolytic Ni-plating [3] were applied to the Mg alloy AZ31 to improve the corrosion fatigue resistance of the alloy. Corrosion fatigue lives and fatigue behavior of the specimens were investigated in detail and their mechanisms will be also discussed. Specific contents in this chapter are summarized as follows.
In section 2 [2], fatigue tests were performed on electroless nickel-plated magnesium alloy specimens in laboratory air and 3% sodium chloride solution. In laboratory air, the effect of surface treatments (plating, blasting and polishing) on the fatigue lives of specimens was found to be minimal. However, in 3% sodium chloride solution, the electroless Ni-plated specimens were found to have shorter fatigue lives than those of the polished and blasted specimens. In order to study the fatigue mechanisms, successive observations of the specimen surfaces were conducted during the fatigue process in both laboratory air and sodium chloride solution. Observations of the fracture surfaces were also conducted to clarify the fatigue mechanism.
In section 3 [3], the fatigue behavior of electrolytically nickel-plated Mg alloy both in laboratory air and in a corrosive environment (3% NaCl) were described. The fatigue

lifetimes, the crack initiation and the propagation behaviors of both plated and unplated specimens were studied in order to determine the effect of a nickel coating. In air, the nickel plating was detrimental because of the easy nucleation of fatigue cracks at depressions in the coating which resulted from the plating process. However, in 3% NaCl, the fatigue properties of plated specimens were markedly superior to those of unplated specimens due to their good resistance to corrosion. Further improvement in the fatigue lives of Ni-plated specimens is expected if the plating process can be modified to eliminate the formation of defects such as surface depressions.

2. Effect of electroless-Ni-Plating on corrosion fatigue behavior of Mg alloy[2]

Dr. Nan performed corrosion fatigue tests on AZ31B magnesium alloy [4], and clarified shorter fatigue lives than those in non-corrosive laboratory air, especially in the lower stress amplitude region. Electroless Ni plating is expected to be beneficial in improving the corrosion fatigue performance of magnesium alloys. However, studies on fatigue behavior of electroless Ni plated magnesium or other alloys have been limited. Punch-Cabrera et al. [5] studied the corrosion fatigue lives of electroless Ni deposited 7075-T6 aluminum alloy in 3% sodium chloride solution. They reported that the deposition increased the corrosion fatigue lives by 60–70% in the low cycle fatigue region of 10^4–10^5 cycles. Contreras et al. [6] reported a remarkable decrease in the fatigue lives of electroless Ni deposited AISI-1045 steel in laboratory air. Saeid et al. [7] investigated the fatigue behavior of electroless Ni deposited Ck45 steel in laboratory air. They also reported that the electroless Ni deposit decreased the fatigue life, because cracks were initiated early during the fatigue process at the interface between the deposit and substrate. Therefore, these results reported to date regarding the effectiveness of electroless Ni deposits on the fatigue lives of alloys are rather different.

In the present study, fatigue tests were conducted on electroless Ni plated AZ31 magnesium alloy specimens in laboratory air and 3% sodium chloride solution, in order to study the effect of electroless Ni plating on fatigue life. For comparison, specimens with different surface treatments, machine-polishing and glass bead-blasting, were also tested. The fatigue mechanisms of the electroless Ni-plated Mg alloy specimens in both laboratory air and 3% sodium chloride solution were studied in detail.

2.1 Specimens and experimental methods

2.1.1 Specimens

The material used in the present study was an extruded AZ31 magnesium alloy. Its chemical composition is listed in Table 1. The main chemical compositions of the material are 3 wt.% aluminum and 1 wt.% zinc. The yield strength, tensile strength, elongation and Young's modulus of the material were found to be 200 MPa, 275 MPa, 11.0% and 45 GPa, respectively. Specimens were machined into a round bar shape with a minimum diameter of 5.6 mm, as shown in Fig. 1.

Wt.(%)								
Al	**Zn**	**Mn**	**Fe**	**Ni**	**Si**	**Pb**	**Ca**	**Mg**
2.98	0.97	0.004	0.007	0.005	0.02	0.01	0.04	Bal.

Table 1. Chemical compositions of the material used

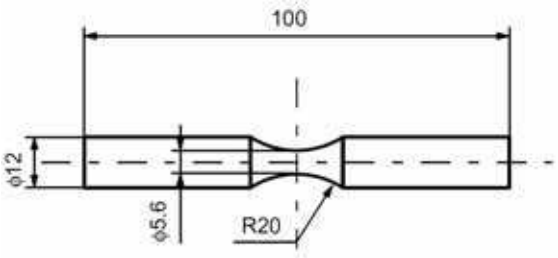

Fig. 1. Shape and dimensions of the specimen (mm).

Solution-pH	Plating time [min]	Plating temperature [K]	Plating bath	Plating thickness [μm]
6.0	60	344	Heat-resistant resin	24

Table 2. Conditions used for electroless Ni-plating

Blasting pressure[MPa]	Blasting distance[m]	Blasting material
0.39	0.1	Glass beads, 150 μm in diameter

Table 3. Conditions employed for glass bead-blasting in the present study

The as-machined specimens were blasted with glass beads, followed by electroless Ni plating prior to the fatigue tests. Tables 2 and 3 show the conditions for the electroless Ni plating and blasting treatments, respectively. Machine-polished specimens were also prepared by polishing the as-machined specimen with emery papers and diamond pastes. Fatigue tests of the glass bead-blasted and machine-polished specimens were conducted for comparison with the electroless Ni plated specimens.

2.1.2 Experimental methods

Fatigue tests were conducted using a cantilever type rotating bending fatigue machine. The tests were conducted at a frequency of 30 Hz, and at an R ratio of − 1. 30 Hz was chosen as a typical frequency, since no significant effect of frequency was observed on the corrosion fatigue behavior within the range of 1–60 Hz. Fatigue tests in laboratory air were conducted at room temperature with humidity of 63–73%.

Corrosion fatigue tests were performed by dripping 3% sodium chloride solution in ion exchanged water onto the specimen surface at a constant rate using a metering pump. The corrosive solution was maintained at a temperature of 298 K. The replica method was used for the successive observations of the specimen surfaces during the fatigue process.

Fatigue tests were interrupted at constant intervals for taking replicas. The collected replicas were examined using an optical microscope with a magnification of 400 times, in order to obtain information regarding crack size and shape during the fatigue process. A part of each specimen was observed directly with an optical microscope to study how cracks propagate and interact with the microstructure of the material. The specimen hardness was measured with a microhardness testing machine under experimental conditions of a 100 g load for 30 s of load time.

2.2 Experimental results

2.2.1 Characterization of the electroless Ni-plated film

Fig. 2(a) shows the cross section of an electroless Ni plated specimen. Good adhesion between the Ni plating film and the magnesium alloy (substrate) is observed, because no abruption was observed along the interface between the plating and substrate, both before and after the fatigue tests. However, sedulous investigation of the interface revealed that local defects are present in the plating film, as shown in Fig. 2(b). The defect density within the plating film was 0.2 per mm. The average thickness of the plated Ni film was 24 μm. The hardness of the plating film was HV_{100} = 487, while that of the magnesium alloy (substrate) was HV_{100} = 57. The latter possesses only 1/8 hardness of the former, indicating a large difference in hardness. Electron probe micro-analysis (EPMA) determined that the chemical composition of the plating film was 92 wt.% Ni and 8 wt.% P.

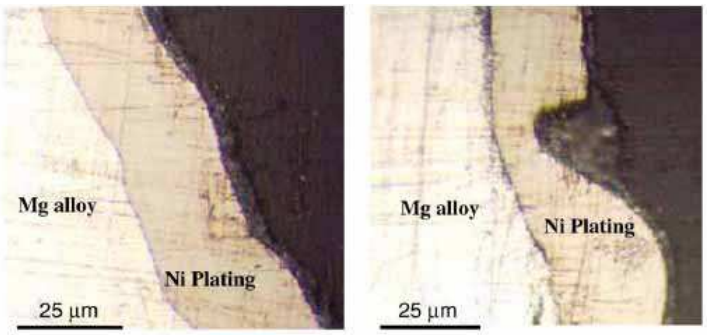

(a) Cross section of the plated specimen (b) Defects in the plating film

Fig. 2. Cross sections of the electroless Ni plated specimen. (a) Cross section of the plated specimen, (b) Defects in the plating film.

2.2.2 Effects of the surface treatments on the fatigue lives

Fig. 3 shows S–N data in laboratory air for the three types of surface treated specimens, polished, blasted, and electroless Ni plated specimens. The solid curve in the figure indicates the approximated S–N curve for the three types of specimens. The dashed line in the figure represents the S–N curve previously reported by the present authors [8] using similar AZ31 magnesium specimens with polished surfaces. The curve was added to make up for limited experimental data of the polished specimen. The dashed line agrees well with the present S–N curve (solid curve) of the specimens with three different surface treatments. Therefore, we can conclude that the S–N data measured in laboratory air are not affected by the surface treatments under the present experimental conditions.

The value of the fatigue limit ranged from 120 to 130 MPa, regardless of the different surface treatments.

Fig. 4 shows S–N curves for the three different type specimens, machine-polished, glass bead-blasted and electroless Ni plated specimens in 3% sodium chloride solution. The solid line in the figure indicates the S–N curve in laboratory air that is shown in Fig. 3.

The corrosion fatigue lives for the polished specimens are equal to those of the blasted specimens. The dashed line in the figure shows the S–N curve for the both polished and blasted specimens. On the other hand, the corrosion fatigue lives for the electroless Ni

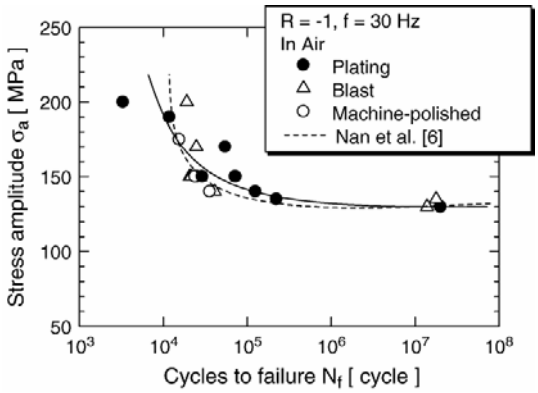

Fig. 3. S–N curves of the plated, polished and blasted specimens in laboratory air. Effect of the surface treatments on fatigue life was minimal in laboratory air.

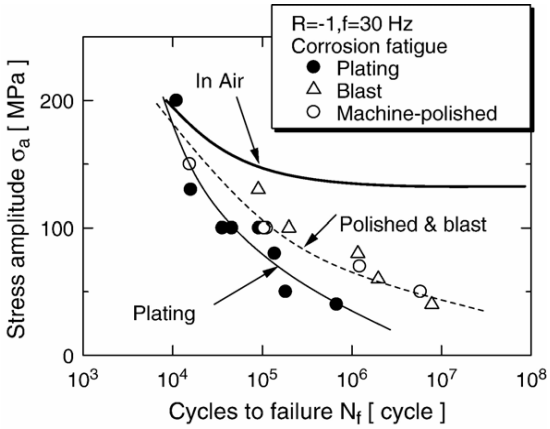

Fig. 4. S–N curves of the plated, polished and blasted specimens in 3% sodium chloride solution. The corrosion fatigue lives of the plated specimens were shorter than the blasted and polished specimens.

plated specimens were shorter than those of the polished and blasted specimens at constant stress amplitudes.

As expected with corrosion fatigue, the fatigue limit disappeared, and significant decreases in the corrosion fatigue lives were observed with the decrease in stress amplitude, regardless of the specimen surface treatment. This observation is common with that of previous studies of other materials, such as steel and aluminum alloy [9, 10].

2.2.3 Successive observations during fatigue process

Fig. 5 shows successive observations for the electroless Ni plated specimen tested in laboratory air at 150 MPa and failed at $N_f = 2.9 \times 10^4$. In these figures, crack initiation is indicated by a solid curve, as it is not so conspicuous due to the rough surface of the plated specimen. Surface irregularities are preeminent in the electroless Ni plated specimen, as a

result of plating particles and surface roughening by the blasting. Fig. 5(b) at N = 6160 cycles, a crack 60 μm in length can be seen on the plated specimen surface. This crack propagated to 240 μm in length at N = 12,320 cycles, as shown in Fig. 5(c). In laboratory air, specimen surface damage such as depressions of the plated surface, which will be later explained in the section on corrosion fatigue, were not observed in these figures.

Fig. 6 shows the results of successive observations of the electroless Ni plated specimen in 3% sodium chloride solution, which was tested at 100 MPa and failed at $N_f = 4.6 \times 10^4$. In Fig. 6(b) at N = 10560 cycles, a 150 μm crack was observed to propagate on the plated specimen surface. This crack propagated to 345 μm in length at N = 15,840 cycles, as shown in Fig. 6(c). During the corrosion fatigue process, a depression of the plated specimen

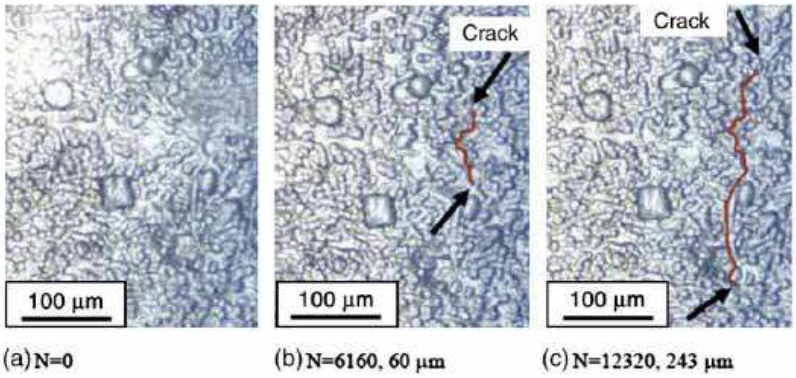

Fig. 5. Successive observations of the electroless Ni plated specimen during the fatigue process in laboratory air tested at stress amplitude 150 MPa ($N_f = 2.9 \times 10^4$). The crack initiated at the specimen surface, as indicated by the arrows.

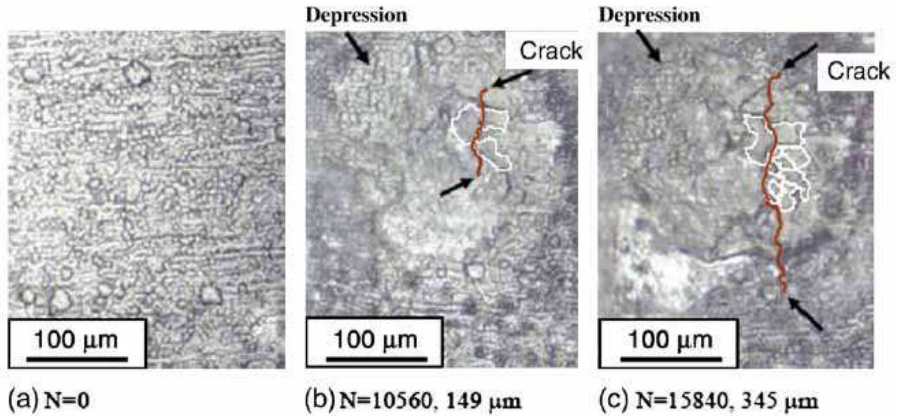

Fig. 6. Successive observations of the electroless Ni plated specimen during the fatigue process in 3% sodium chloride solution tested at stress amplitude 100 MPa ($N_f = 4.6 \times 10^4$). A depressed portion appeared on the specimen surface, and a crack initiated within the depressed area.

surface (ca. 270 μm diameter) was observed as indicated in the figures. The mechanism for the depression of the plated specimen surface is discussed later.

2.2.4 Crack propagation behavior

Fig. 7(a) shows the crack propagation curves in laboratory air at a stress amplitude of 150 MPa for both the electroless Ni plated and the polished specimens. There is little difference observed between the crack propagation curves of both specimens. Fig. 7(b) shows the crack propagation curves in sodium chloride solution at a stress amplitude of 100 MPa for both the electroless Ni plated and the polished specimens. A crack is initiated earlier in the electroless Ni plated specimen than in the polished specimen. This shortening in the crack initiation corresponds well with the experimental finding that the corrosion fatigue lives of the electroless Ni plated specimens became shorter than those of the polished specimens.

Figs. 8(a) and (b) show the relations between the crack propagation rate da/dN (m/cycle) and the stress intensity factor range ΔK (MPa $m^{1/2}$) in laboratory air and sodium chloride solution, respectively. ΔK was calculated as $1.04\times0.73\sigma_a\sqrt{\pi a}$, where σ_a is the stress

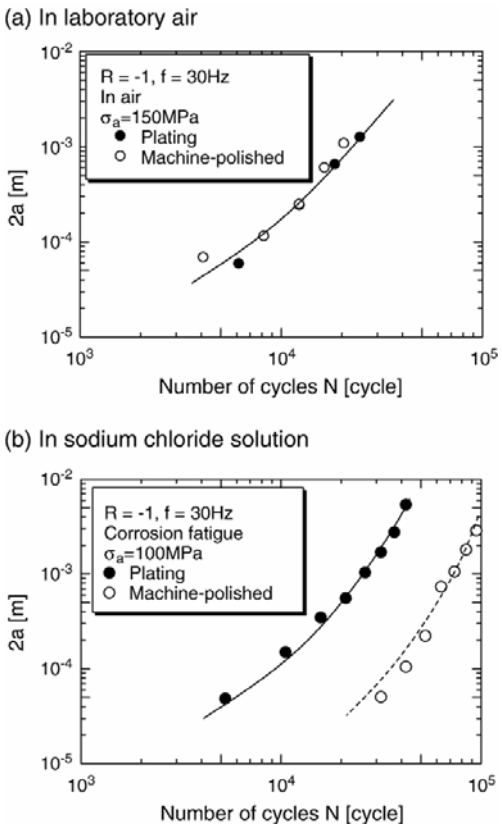

Fig. 7. Crack growth curves (2a-N) in corrosive environments, where 2a is the crack length and N is the number of loading cycles. (a) In laboratory air. (b) In sodium chloride solution.

amplitude, a is a half crack length, 1.04 is the stress concentration factor for the notch introduced in the specimen. 0.73 is a modification factor for assuming a crack shape as a half circular one. As can be seen from these figures, no differences in the relations of da/dN-ΔK between the electroless Ni plated and the polished specimens are seen for either conditions of laboratory air or sodium chloride solution. The solid curves shown in these figures indicate the approximated curves of the da/dN-ΔK relation.

2.2.5 Fractography

Fig. 9 shows the fracture surface of an electroless Ni plated specimen failed at 2.22×10^5 cycles and a stress amplitude of 135 MPa in laboratory air. The semi-circular shaped fatigue crack, as indicated by the dotted line in the figure, which may have started from the specimen surface, can be seen on the fracture surface of the plated specimen. In the polished

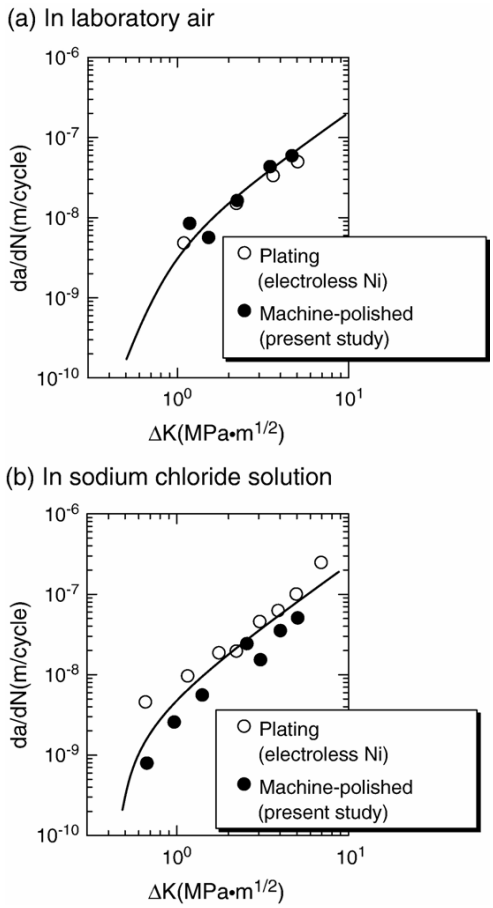

Fig. 8. Relationship between the crack propagation rate da/dN and the stress intensity factor range ΔK for the electroless Ni plated and polished specimens. (a) In laboratory air. (b) In 3% sodium chloride solution.

specimen, a similar semi-circular shaped fatigue crack initiated from the specimen surface was also observed on the fracture surface. Other plating damage, such as the depression or detachment of the plating film was not observed. This indicates that good cohesion was maintained during the fatigue process in laboratory air. The above observation corresponds well with the fact that plating depressions were not seen during the successive observations in laboratory air (Fig. 5).

Fig. 10 shows a fracture surface of the electroless Ni plated specimen that failed in sodium chloride solution at 9×10^4 cycles and a stress amplitude of 100 MPa. Unlike with laboratory air, a corrosion pit was initiated in sodium chloride solution at the interface between the plating film and the substrate, as indicated in the figure. The corrosion pit diameter was estimated as 300 μm. This estimated diameter is almost equivalent to the diameter of the plating depression shown in Fig. 6. The fatigue crack initiated from the bottom of the corrosion pit as indicated in the figure, and then caused the final failure of the specimen.

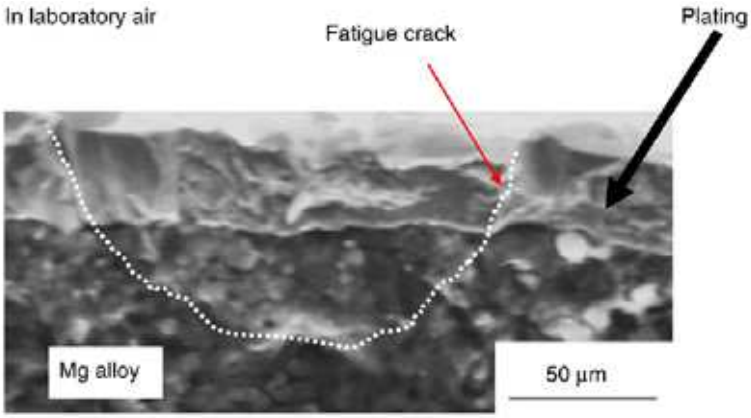

Fig. 9. Fracture surface of the electroless Ni plated specimen, failed at 2.23×10^5 cycles and stress amplitude of 135 MPa in laboratory air.

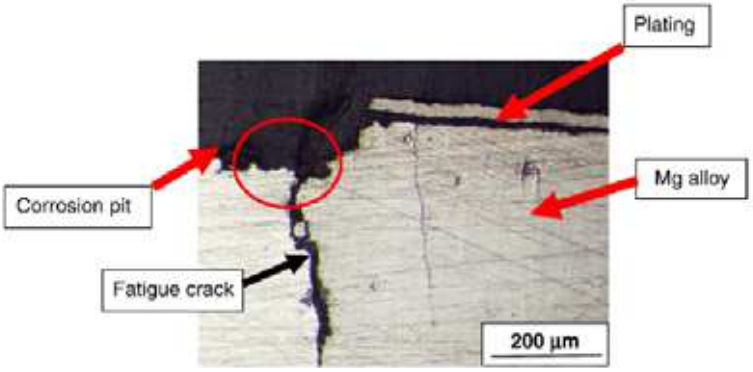

Fig. 10. Fracture surface of the electroless Ni plated specimen, failed at 9×10^4 cycles and stress amplitude of 100 MPa in sodium chloride solution.

2.3 Discussion

2.3.1 Comparison between the fatigue lives in laboratory air and those in sodium chloride solution

As shown in Fig. 4, the corrosion fatigue lives in sodium chloride solution were shortened compared with those in laboratory air. This shortening of the corrosion fatigue lives was observed regardless of the specimen treatment; polished, blasted or electroless Ni plated. However, the worst case was the electroless Ni plated specimens.

During the corrosion fatigue process, corrosion pits were initiated at the specimen surface (polished and blasted specimens) or the interface between the plating and the Mg alloy (electroless Ni plated specimen). A crack was initiated from the bottom of the corrosion pit that reached a critical depth for crack initiation, as shown in Fig. 10, then propagated and was followed by final failure of the specimen.

On the other hand, in laboratory air, cracks were initiated from the surface defects, for example, from nonmetallic inclusions or slip lines on the specimen surface of the polished and blasted specimens. This might also be true for the case of the electroless Ni plated specimen, because differences in the crack initiation and propagation behavior were not observed between the electroless Ni plated and the polished specimens, as shown in Fig. 7(a). The fatigue crack may initiate from the surface of the plating film.

With regard to crack propagation behavior, comparison of the $da/dN-\Delta K$ relation in laboratory air (Fig. 8(a)) and in 3% sodium chloride solution (Fig. 8(b)) revealed no differences in crack propagation.

Therefore, the corrosion fatigue lives of the three different specimens were shortened in sodium chloride solution compared to laboratory air, because the crack initiation processes were hastened due to the initiation and growth of corrosion pits.

2.3.2 Corrosion fatigue lives of the electroless Ni plated specimens

The corrosion fatigue lives of the electroless Ni plated specimens became shorter than those of the polished and blasted specimens.

In general, compressive residual stresses are introduced to the specimen surface by electroless Ni plating or blasting treatment [11-13] Roughening of the specimen surface is also induced by the blasting treatment. Compressive residual stresses are known to improve the fatigue strength. On the other hand, surface roughening has a negative effect on the fatigue strength, because it hastens crack initiation.

As can be seen from Fig. 3, the S–N curves in laboratory air were not affected by the specimen surface treatments of electroless Ni plating, polishing or blasting. This indicates that the compressive residual stresses and surface roughening, which might be introduced into the specimens by plating and blasting, were not sufficiently large to affect the fatigue lives of both types of specimens.

Therefore, another mechanism, other than compressive residual stresses and surface roughening, is required to explain the lower corrosion fatigue strength of the electroless Ni plated specimens compared with those of the blasted and polished specimens.

Fig. 11 shows an SEM (scanning electron microscopy) photograph of the electroless Ni plated specimen surface. Small plural pores are seen to be initiated on the specimen surface as indicated by the arrows in the figure. Fig. 12 shows a cross section of the electroless Ni plated specimen in sodium chloride solution, which was tested and interrupted at half of the fatigue life. A corrosion pit initiates at the interface between the plating film and the substrate as indicated in the figure. During the corrosion fatigue process, it is considered

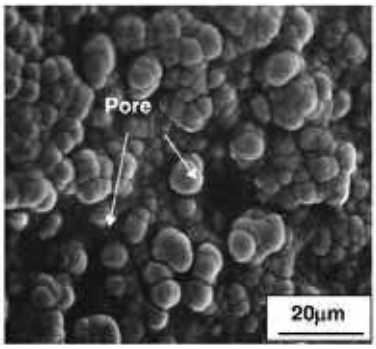

Fig. 11. SEM photograph indicating the specimen surface morphology of the electroless Ni plated specimen.

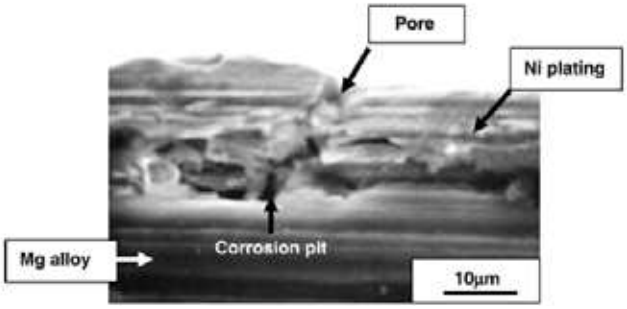

Fig. 12. Cross section of the electroless Ni plated specimen, which was tested and interrupted during fatigue in sodium chloride solution. The corrosion pit is found to be initiated at the interface between the plating and the matrix.

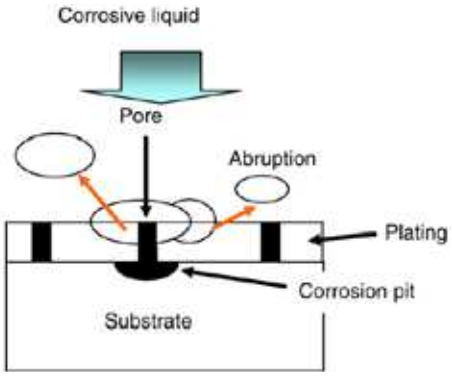

Fig. 13. Schematic illustration showing the mechanism for abruption of the plating membrane in sodium chloride solution.

that the corrosive solution infiltrates to the interface through the small pores indicated in Fig. 12, and this leads to local corrosive reactions.
Fig. 13 shows a schematic illustration of the mechanism for the depression and abruption of the plating film during the corrosion fatigue process. Firstly, corrosive solution infiltrates to the interface through the small pores during the corrosion fatigue process. Then, the pH value decreases and leads to local corrosive reaction at the interface, followed by the initiation and growth of the corrosion pit. A crack
The results, as validated by Fig. 7(b), indicate that the corrosion fatigue lives of the initiates at the bottom of the corrosion pit and leads to the final failure of the specimen. The depression and abruption of the plating film might be induced at the location where the corrosion pit initiated and grew. With regard to the crack propagation behavior, no significant differences were observed, for the various surface treatments, in either laboratory air or sodium chloride solution, as shown in Fig. 8, electroless Ni plated specimens became shorter than those of the polished and blasted specimens primarily due to the acceleration of the crack initiation process in the electroless Ni plated specimens.

3. Corrosion fatigue resistance of an electrolytically-plated Mg alloy [3]

Surface treatments, such as coating or plating of the material surface have been examined for enhancement of the corrosion fatigue resistance of magnesium alloys, and in general they have not been successful. For example, Khan et al. [14, 15] found no effect on the fatigue properties of anodized AM60 Mg alloy tested in 55% humidity and 80% humidity environments. Eifert and Thomas [16] also investigated the effect of anodizing on the fatigue performance of WE43A-T6 Mg alloy in laboratory air and found that anodizing decreased the fatigue strength by 10% in the high cycle regime. Such results are not surprising since anodized coatings are not impervious to moisture. In addition, Ishihara et al. [2] found that an electroless-nickel plating had no beneficial effect on the corrosion fatigue behavior of AZ31 magnesium alloy.
There have been a few investigations involving the surface treatment of base materials other than magnesium which have been successful in improving resistance to corrosion fatigue. For example, Puchi-Cabrera et al. [5] found the fatigue life of 7075-T6 aluminum alloy plated with electroless-nickel and tested in a 3% NaCl solution to be 60–70% higher relative to the unplated condition. Asquith et al. [17] studied the aluminum alloy 2024 which had been subjected to both a coating developed by plasma electrolytic oxidation (PEO) and shot peening. The surface treated alloy was tested in laboratory air. They reported that the double surface treatment resulted in an improvement in fatigue life.
On the other hand, Contreras et al. [6] found the fatigue life of AISI-1045 carbon steel coated with an electroless-nickel plating and tested in an ambient atmosphere to be significantly reduced. A similar result was reported by Saeid et al. [7] for CK45 carbon steel plated with an electroless-Ni coating. In this case the reduction in fatigue life was attributed to early crack initiation at the interface between the matrix and the plating. Cirik and Genel [18] studied the effect of varying thickness of an anodic coating on 7075 aluminum alloy in laboratory air, and found that the anodic coating reduced the fatigue strength.
As reviewed above, a number of investigations of surface-coating methods for the improvement of fatigue strength have been conducted, and in particular case of magnesium alloys none of approaches cited above has been shown to be beneficial. In addition, the fatigue crack initiation and propagation behavior of surface treated specimens have not been examined in any detail.

In the present investigation the influence of a protective barrier coating of nickel, which is electrochemically much more noble than magnesium, on the corrosion fatigue properties of a magnesium alloy, AZ31B, will be examined. In addition, the fatigue crack initiation and crack growth processes will be studied using a replica technique.

3.1 Specimens and experimental procedures

3.1.1 Specimens

a. Materials

The chemical composition and mechanical properties of the commercially-available extruded AZ31B magnesium alloy used in the present study are listed in Table 1 and Table 2, respectively. The main chemical components of the alloy are Al (3 wt.%) and Zn (1 wt.%). The balance is Mg together with trace amounts of other elements.

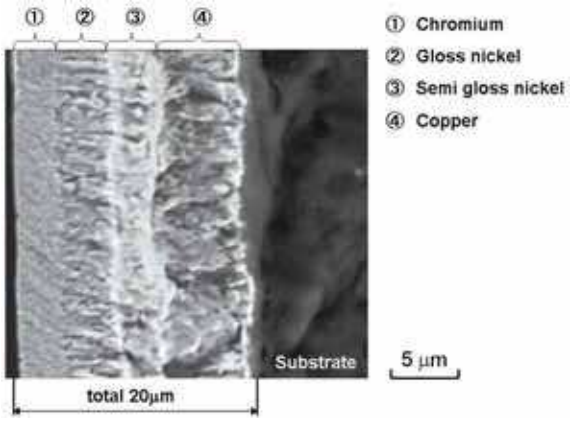

(a) Cross section of the plated film.

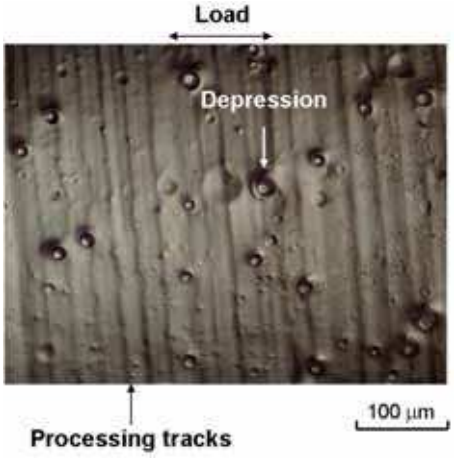

(b) Plated specimen surface.

Fig. 14. Optical micrographs of the plated film.

b. Unplated specimens

Round bar rotating bending fatigue specimens with a minimum diameter of 5.6 mm were machined from the as-received round bar (ϕ15 mm). Prior to testing the as-machined specimen surfaces of the gauge section of specimens were polished with 400–2000 emery-papers and then with diamond paste with grit size of 1 μm to obtain a mirror-like finish (roughness: 0.07 μm). The stress amplitude applied to the specimen was calculated by multiplying the nominal stress by a stress concentration factor of 1.02.

c. Plated specimens

The plated specimens were prepared by cleaning the as-machined specimens in alkali solution, followed by the application of a 20 μm – thick multilayer-electrolytic coating. The plating was conducted at conditions, pH: 4–5, temperature: 318–328 K, and current density: 3–5 A/dm^2. The detailed plating procedures were as follows:

1. *Bath compositions*: nickel sulfate, nickel chloride, and acidum boricum.
2. *Plating times*: total 30 min including degreasing.
3. *Additive*: the brightening agent (gloss agent) was added to improve the plating quality.

Fig. 14a shows a cross section through the multi-layered coating which consists of an inner 7–8 μm layer of copper, two 4–5 μm intermediate layers of nickel (semi-gloss and gloss nickel) and an outer 3 μm layer of chromium. The outer chromium layer on the specimen surface was applied for the purpose of improving the surface finish and for providing additional corrosion protection. The gloss and semi-gloss nickel layers are applied to improve a surface finish, and to get a good adhesiveness to the substrate, respectively. The inner copper layer on the substrate was applied for the purpose of improving adhesiveness of the film to the substrate.

Fig. 14b shows the specimen surface of a plated film. Many circular depressions (a real density: 28 mm^2) with diameters from 10 to 100 μm are present on the plated surface. These depressions are assumed to have been generated by hydrogen gas evolution during the plating process; however, the detailed mechanism of depression formation is unknown at present. In addition to depressions, small bumps (protuberances) were also formed, Fig. 14A.

3.1.2 Experimental procedures

Rotating bending fatigue tests were conducted in the frequency range of 10–30 Hz in laboratory air at room temperature and with a relative humidity of 68%. Fatigue tests of unplated specimens were carried out in air and in 3% NaCl solution. Fatigue tests on plated specimens were carried out in these two environments plus additional tests in purified water. Prior studies [19] have shown that a dripping process of the NaCl solution onto the specimen surface was more detrimental to corrosion fatigue properties than was a total immersion process, due to the greater supply of oxygen which in turn increases the rate of the cathodic reduction. This dripping process was used in the present investigation. The solution was dripped onto the specimen surface during cyclic loading at a constant rate of 3.67 g/min.

The replica method was used for the successive (continuous) observations of the specimen surface during the fatigue processes of the unplated and plated specimens. Fatigue tests were interrupted periodically to obtain replicas of the specimen surfaces at a constant interval of cycles, ΔN. The interval was usually 5–7% of the total fatigue life N_f. Thus, a total of 15–20 replicas were collected for one fatigue test. The replicas enable measurement of the crack length during the fatigue crack growth process. It is considered that the replication did not affect the corrosion fatigue behavior or mechanism, since the corrosion fatigue lives were not changed so much with or without employing the replica.

An optical microscope (Olympus-BX51 M) was used to examine the replicas. When a fatigue crack was clearly identified on one of the later replicas, the earlier replicas were re-examined to determine the earliest fraction of life at which a fatigue crack could be identified. Micrographs of the cracks were obtained using a camera system (Olympus-DP12). A crack propagation curve was constructed by plotting the crack lengths $2a$, measured as a function of the number of cycles N. In addition, the fracture surfaces were observed using a scanning electron microscope (SEM; Hitachi High-Technologies, TM-1000).

3.2 Experimental results

3.2.1 Effect of electrolytic coating on the fatigue life in laboratory air and in corrosive environments

Fig. 15(a) shows stress–cycle (S–N) curves of the unplated specimens in laboratory air and in a corrosive environment (3% NaCl solution). The solid and broken lines in the figure have been approximately fitted to the experimental results. As can be seen from the figure, the corrosion fatigue lives of unplated specimens are significantly decreased in 3% NaCl,

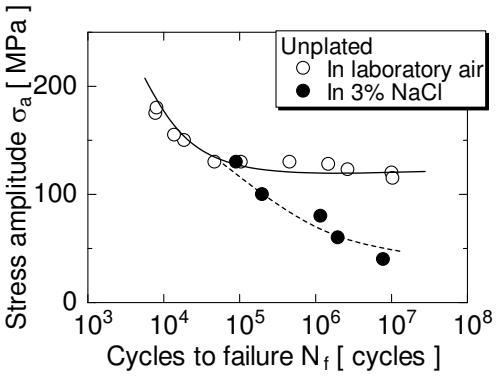

(a) Unplated specimens.

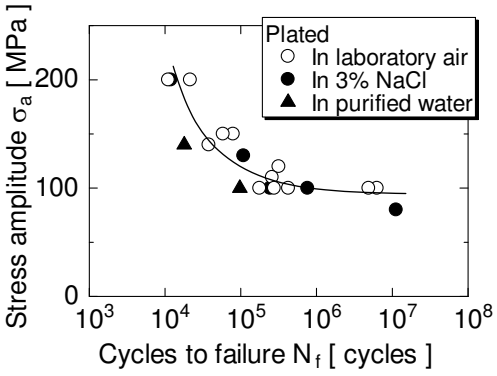

(b) Plated specimens.

Fig. 15. Effect of environment on the S–N curves for both (a) unplated specimens and (b) plated specimens.

especially in the low stress amplitude region. In air, fatigue cracks initiated at surface inclusions; in 3% NaCl, fatigue cracks initiated at corrosion pits which were responsible for the large decrease in fatigue strength relative to air [20]. Fig. 15(b) shows *S–N* curves of the electrolytically-plated specimens in laboratory air and in the purified water and the in the 3.5% NaCl environments. It is noted that for the plated specimens no significant effect of environment was found, a demonstration of the protective behavior of the coating. However, in comparison with Fig. 15(a), the fatigue strength of the plated specimens in air is less than of the unplated specimens.

3.2.2 Successive observations during the fatigue processes

Fig. 16A shows the results of successive observations of the plated specimen surface during the fatigue process in laboratory air at a stress amplitude of 140 MPa as obtained by the replica technique. The fatigue life, N_f, at this stress amplitude was 38,700 cycles. Fig. 16A-a shows that the specimen surface prior to fatigue loading (N = 0) contained a semi-spherical depression which was 54 μm in diameter and 15 μm in depth. After cyclic stress loading at N = 6000 cycles (15% of life), a crack had already initiated from at the bottom of the depression, as indicated by the arrow in Fig. 16A-b. At 10,000 cycles, the crack had propagated to a length of 250 μm (Fig. 16A-c). The fracture surface of this specimen in the area of crack initiation is shown in Fig. 17b, and some debonding between the outer chromium and the nickel layer can be seen.

Fig. 16B shows the results of successive observations of the plated specimen surface during the corrosion fatigue process in purified water at a stress amplitude of 140 MPa. In this case the fatigue life was N_f = 17,911 cycles. An elliptically-shaped bump was present on the specimen surface, and is indicated by the dashed curves in the figure. This bump is believed to have been created during the plating process. As revealed by subsequent examination, an

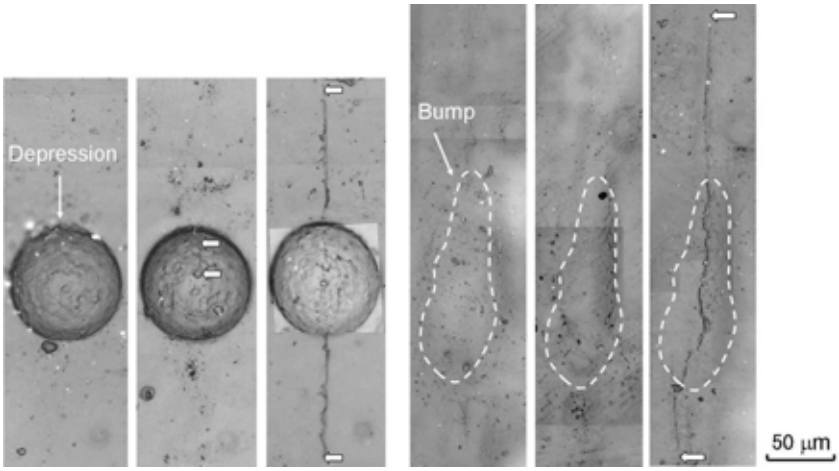

A B

(a) N=0 (b) N=6000 (c) N=10000 (a) N=0 (b) N=1500 (c) N=3000

Fig. 16. Successive observations of the plated surface during the fatigue process in [A] laboratory air and [B] in purified water, at a stress amplitude of 140 MPa.

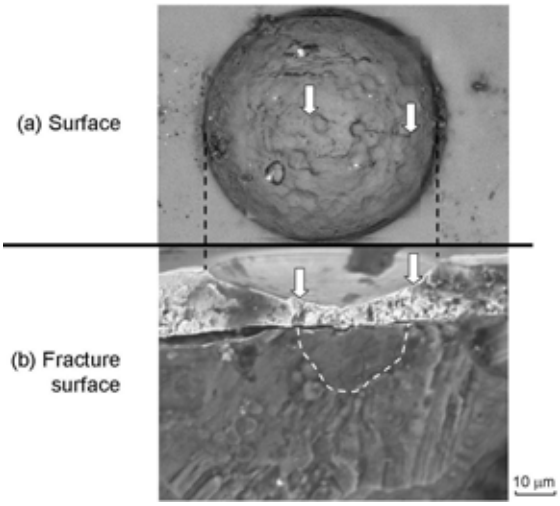

Fig. 17. Fracture surface of the plated specimen (in laboratory air, σ_a = 140 MPa, N_f = 38,700 cycles).

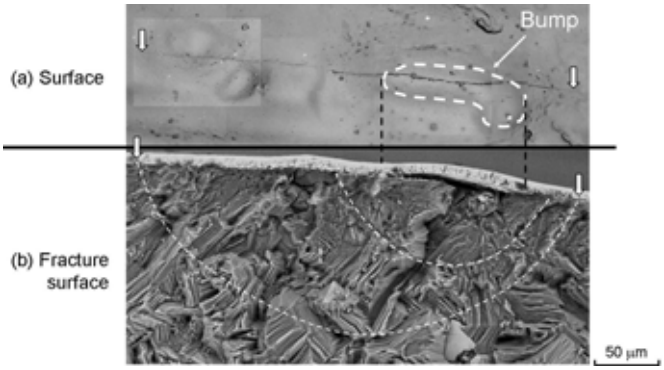

[A] In laboratory air, σ_a=100 MPa, N_f=177049 cycles. Arrows indicate crack tips.

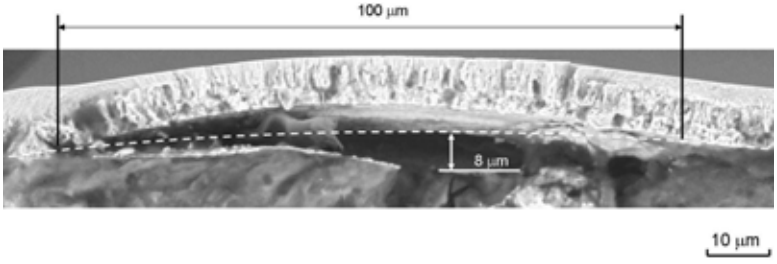

[B] Magnification of the bump shown in Fig. 18[A].

Fig. 18. Fracture surface of the plated specimen (in laboratory air, σ_a = 100 MPa, N_f = 177,049 cycles).

irregularly-shaped depression was found below this bump, at the interface between the copper and the substrate. At 1500 cycles, no crack was observed at the surface at the bump, Fig. 16B-b. However, at 3000 cycles, a crack of a length of 300 μm appeared suddenly on the specimen surface at the location of the bump, Fig. 16B-c.
In all of the fatigue tests of plated specimens, fatigue cracks were found to initiate either at a depression (SN-type) or at a bump (IN-type), regardless of the environment.
Fig. 17a shows a crack initiated at a depression at 16% of life. Fig. 17b shows the subsequent fracture surface at this location.
Fig. 18 shows combined micrographs of the surface and fracture surface of the plated specimen which had been tested in laboratory air. The specimen had been cyclically loaded at a stress amplitude of 100 MPa until failure at 177,049 cycles.
A crack initiated from the bottom of the depression located along the interface between the copper layer and the substrate, and then propagated along the surface and into the specimen. The depression is located just beneath a bump. Fig. 18B shows a magnified micrograph of Fig. 18a indicating the appearance and size of the depression (100 μm long and 8 μm deep). The stress concentration due to the geometry may have promoted crack initiation at the bottom of the depression.

3.2.3 Crack propagation behavior

Fig. 19a and b shows the relations between crack length ($2a$) vs. the number of stress cycles (N) and $2a$ vs. fatigue life ratio (N/N_f), respectively, where N_f is the total fatigue life. The

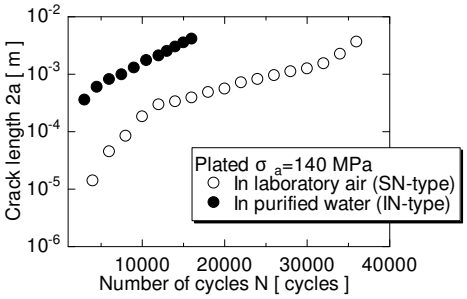

(a) 2a vs. N.

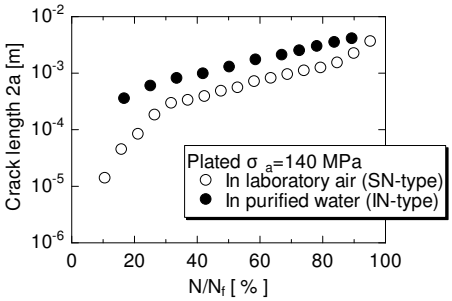

(b) 2a vs. N/N_f.

Fig. 19. Crack propagation behavior for plated specimens at a stress amplitude of 140 MPa. Crack length ($2a$) as a function of (a) the number of stress cycles (N), and (b) the fatigue life ratio (N/N_f).

fatigue processes of plated specimens were measured in laboratory air and in purified water at a constant stress amplitude of 140 MPa. When several cracks initiated during the fatigue process, the crack length for the main crack which led to final failure of the specimen was plotted.

For the plated specimen, the crack (SN-type) was initiated early at 10% of the fatigue life during the fatigue process, which indicates that the total fatigue life of the plated specimen is almost equal to the crack propagation life. However, for the IN-type plated specimen, a crack with a length of 200 μm suddenly appeared on the specimen surface at N/N_f equal to 20%. The crack in the IN-type specimen is also expected to initiate early during the fatigue process, as for the SN-type specimen, because the crack propagation curves and fatigue lives of both specimens are almost the same.

Three-dimensional finite element analysis was conducted using commercial software, Ansys, to study stress distribution around the depression. The analysis revealed that stress concentration factor for the present depression was 2.1, and the distance over which the dominant stress falls off to nil stress concentration was about 90 μm from the center of the depression. The value of the stress concentration factor was also estimated as, k = 2.13 [21] by considering the notch shape and sizes appearing in Fig. 17. These results suggest that in the SN-type specimen, the rate of crack propagation accelerated in the region of $2a$ < 180 μm, due to the effect of stress concentration at the semi-spherical notch (SN-type), while in the region $2a$ > 180 μm, no acceleration in the rate of crack propagation occurred, because the location of the crack tip deviated from the area influenced by the stress concentration. In addition to the above notch effect, effect of crack geometry (a depression) on crack closure and local chemistry is also considered to be important factors influencing the above crack propagation behavior. Further study is needed to clarify these issues.

Fig. 20 shows log–log plot of the rate of crack propagation da/dN (m/cycle) and the stress intensity factor range ΔK (MPa $m^{1/2}$) for the plated specimens in laboratory air and purified water. Eq. (1) was used to calculate ΔK, where the value of 0.73 was introduced with the assumption that the crack shape is a semi-circular [22]. In Fig. 20, the stress concentration at the notch, as discussed in Fig. 19, was not taken into a consideration in the calculation of ΔK, since an exact solution for stress intensity factor (SIF) of the crack emanating from the depression is not available at present. The relationships of da/dN vs. ΔK in laboratory air and in purified water are almost the same, in other words, the environmental effects have no influence on the relationship at the rate of the crack propagation, above 10^{-9} m/cycle. Environmental effect is expected to exist at the region of the lower rate of the crack propagation. Nan et al. [20] investigated the rate of crack growth of the extruded AZ31 Mg alloy in laboratory air and 3% sodium chloride solution. They reported that in the rate of the crack growth, above 10^{-9} m/cycle, there is no acceleration due to the corrosive environment. A similar result was also reported by Khan et al. [14, 15] in the study of Mg alloy. They studied the rate of crack propagation under the low (55%) and the high (80%) humidity in laboratory air. At the rate of crack growth above 10^{-9} m/cycle, effect of the atmosphere humidity on the rate of crack propagation was not observed.

$$\Delta K = 0.73\sigma_a\sqrt{\pi a} \tag{1}$$

The relationship between da/dN and ΔK is expressed by Eq. (2):

$$da/dN = 6.5\times10^{-9}(\Delta K - 0.45)^2 \tag{2}$$

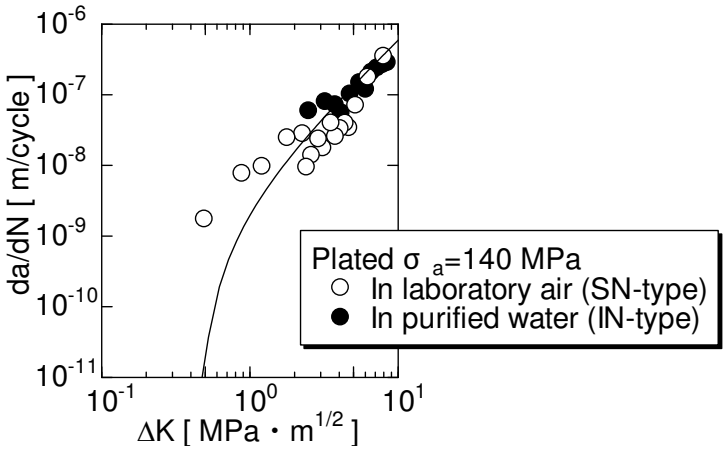

Fig. 20. Relationship between the crack propagation rate da/dN, and the stress intensity factor range ΔK, for the Ni-plated specimen.

3.3 Discussion

3.3.1 Fatigue mechanism of the Ni-plated specimen

Experimental observations revealed that two types of crack initiation mechanism occur in the plated specimens, as schematically illustrated in Figs. 21a (SN-type) and b (IN-type). In both cases, under repeated loading, a crack initiates at the bottom of the depression, where stress concentration occurs. The crack then propagates in the direction of the substrate, which leads to the final failure of the specimen.

These semi-spherical depressions and cavities were observed to be present prior to fatigue loading, and therefore they are assumed to be introduced into the specimen by hydrogen gas evolution during the plating process. For investigating effect of hydrogen gas on the fatigue life of the material, the following experiment was conducted. After plating, the

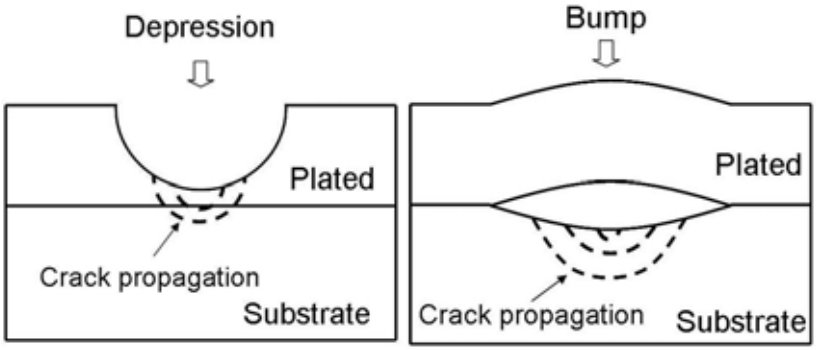

(a) SN-type (b) IN-type

Fig. 21. Schematic illustration of the fatigue mechanism for the Ni-plated specimens: (a) SN-type and (b) IN-type.

specimens were heated in a furnace at 523 K for 2 h, to eject atomic hydrogen stored inside of the specimen. Then the fatigue life of the heated specimen was compared with the one for the unheated specimen. The comparison showed no effect of the heating. So, it is considered that the effect of the atomic hydrogen on the fatigue life is not pronounced enough to affect the fatigue life.

The fatigue mechanisms of the plated specimens are expected to be the same, regardless of the environment, because the fatigue life in laboratory air and in 3% NaCl solution (or in purified water) are in good agreement with each other, as shown in Fig. 15b. The fatigue limit for the plated specimen is slightly decreased compared with that for the unplated specimen in laboratory air, Fig. 15. This is because depressions or cavities act as crack initiators during the fatigue process. The fatigue life of the Ni-plated specimen will be improved by the elimination of surface or interface depressions.

3.3.2 Corrosion fatigue resistance of the electrolytically-plated magnesium alloy

In the case of the electroless plated specimen reported by Ishihara et al. [2], small holes were introduced in the plating-film during the plating process. In the corrosive environment, corrosive liquid reached the substrate through these small holes, and generated the corrosion pit at the interface between the plating-film and the substrate. Early crack initiation and shorter fatigue life were induced by the corrosion pit formation. However, in the present Ni-based electrolytic plated specimen, the plating-film is thought to prevent direct contact between Mg substrate and corrosive liquid during the corrosion fatigue process, due to dense and sound plating-film, Fig. 14. A measurement of polarization curve revealed that corrosion current density for the present Ni-based electrolytic plated specimen was 0.18 A/m^2, which is lower than 0.73 A/m^2 for the electroless plated specimen. The result indicates that the corrosion resistance of the former is superior to the latter. This is the main reason why the fatigue lives of the Ni-based electrolytically-plated specimen were not affected by the corrosive environment, as shown in Fig. 15b.

4. Conclusions

Fatigue tests were performed in laboratory air and in corrosive environments using Mg alloy AZ31 specimens with two types of plating, i.e. electroless Ni-plating and electrically Ni-plating. The following conclusions were obtained:

[A] Electroless Ni-Plating:

Fatigue tests were conducted in laboratory air and 3% sodium chloride solution using three types of surface treated specimens, machine-polished, glass bead-blasted and electroless Ni plated Mg alloy specimens. The following conclusions were reached.

1. In sodium chloride solution, fatigue lives were significantly lowered compared with those in laboratory air, regardless of the three types of specimen treatment.
2. In laboratory air, the S–N curves were not affected by the specimen surface treatments. On the other hand, the corrosion fatigue lives for the electroless Ni plated specimens became shorter than those for the polished and blasted specimens at constant stress amplitudes. The corrosion fatigue lives for the polished specimens were almost the same as those for the blasted specimens.

3. No significant differences in crack propagation behavior due to the different surface treatments were observed in either laboratory air or sodium chloride solution. The rates of crack propagation were almost the same for measurements in both laboratory air and sodium chloride solution.
4. Corrosive solution infiltrated to the interface through the small pores within the plating film during the corrosion fatigue process. This led to local corrosive reactions at the interface, and corrosion pits were initiated. Cracks were initiated at the bottom of the corrosion pits and propagated, leading to the final failure of the specimen. The corrosion fatigue lives of the electroless Ni plated specimens became shorter than those of the polished and blasted specimens, primarily because of the acceleration of the crack initiation process in the electroless Ni plated specimens.

[B] Electrolytically Ni-Plating:

1. The corrosion fatigue lives of the Ni-plated specimens were almost the same as those measured in laboratory air, which indicated a beneficial effect of electrolytic Ni-plating to protect Mg alloys from damage due to corrosion fatigue.
2. Two types of crack initiation sites were found in the Ni-plated specimens, regardless of the test environment. Cracks were initiated from depressions on the specimen surface (SN-type), or from depressions located along the interface between the substrate and plate, i.e., between magnesium alloy and copper (IN-type).
3. The SN-type crack was initiated early during the fatigue process in the Ni-plated specimen, at 10% of the fatigue life. For the IN-type Ni-plated specimen, a crack with a length of 200 μm suddenly appeared on the specimen surface at N/N_f equal to 20%.
4. The fatigue life of the Ni-plated specimen will be improved by the elimination of surface or interface depressions which are introduced during the plating process.

5. Acknowledgements

These studies were performed under a grant from JSPS (NO. 20560069). The authors express their thanks to JSPS. In addition, they thank Takamatsu Plating Co. Ltd., for providing financial support during the course of the present study.

6. References

[1] Y. Kojima, Handbook advanced magnesium technology, Kallos Publishing Co. Ltd., Tokyo (2000).

[2] S. Ishihara, H. Notoya, A. Okada, Z. Y. Nan and T. Goshima, Effect of electroless-Ni-plating on corrosion fatigue behaviour of magnesium alloy ,*Surface coating technology*, Vol.202, pp.2085-2092, 2008.

[3] S. Ishihara, T. Namito, H. Notoya, A. Okada, and T. Goshima, Corrosion fatigue resistance of magnesium alloy with electrolytic Ni-plating, *International Journal of Fatigue*, Vol.32, pp. 1299-1305, 2010.

[4] Z. Y. Nan, PhD thesis, University of Toyama, 2005.

[5] E.S. Puchi-Cabrera, C. Villalobos-Gutiirrez, I. Irausqumn, J. La Barbera-Sosa and G. Mesmacque, Fatigue behavior of a 7075-T6 aluminum alloy coated with an electroless Ni–P deposit, *Int J Fatigue* 28 (12) (2006), pp. 1854–1866.

[6] G. Contreras, C. Fajardo, J.A. Berríos, A. Pertuz, J. Chitty and H. Hintermann *et al.*, Fatigue properties of an AISI 1045 steel coated with an electroless Ni–P deposit, *Thin Solid Films* 355–356 (1999), pp. 480–486.

[7] T. Saeid, S. Yazdani and N. Parvini-Ahmadi, Fatigue properties of a Ck45 steel coated with a post-heat treated Ni–Cu–P electroless deposit, *Surf Coat Technol* 200 (20–21) (2006), pp. 5789–5793.

[8] Z.Y. Nan, S. Ishihara, T. Goshima and R. Nakanishi, Scanning probe microscope observations of fatigue process in magnesium alloy AZ31 near the fatigue limit, *Scr Mater* 50 (4) (2004), pp. 429–434.

[9] S. Ishihara, S. Saka, Z.Y. Nan, T. Goshima and S. Sunada, Prediction of corrosion fatigue lives of aluminum alloy on the basis of corrosion pit growth law, *Fatigue Fract Eng Mater Struct* 29 (2006), pp. 472–480.

[10] S. Ishihara, S. Saka, Z.Y. Nan, T. Goshima, H. Shibata and B.L. Ding, Study on the pit growth during corrosion fatigue of aluminum alloy, *Int. J. Mod. Phys. B* 20 (25,26 & 27) (2006), p. 3975.

[11] J.A. Diaz, M. Passarrelli, J.A. Berrios and E.S. Puchi-Cabrera, Fatigue behavior of a 4340 steel coated with an electroless Ni-P deposit, *Surf. Coat. Technol.* 149 (2002), p. 45.

[12] Rajan Ambat and W. Zhou, Electroless nickel-plating on AZ91D magnesium alloy: effect of substrate microstructure and plating parameters, *Surf. Coat. Technol.* 179 (2004), p. 124.

[13] J.Y. Song and Jin Yu, Residual stress measurements in electroless plated Ni–P films, *Thin Solid Films* 415 (2002), p. 167.

[14] S. Alam Khan, Y. Miyashita, Y. Mutoh and T. Koike, Effect of anodized layer thickness on fatigue behavior of magnesium alloy, *Mater Sci Eng A* 474 (2008), pp. 261–269.

[15] S. Alam Khan, Y. Miyashita, Y. Mutoh and T. Koike, Fatigue behavior of anodized AM60 magnesium alloy under humid environment, *Mater Sci Eng A* 498 (2008), pp. 377–383.

[16] A.J. Eifert and J.P. Thomas, Influence of anodization on the fatigue life of WE43A-T6 magnesium, *Scripta Mater* 40 (8) (1999), pp. 929–935.

[17] D.T. Asquith, A.L. Yerokhin, J.R. Yates and A. Matthews, Effect of combined shot-peening and PEO treatment on fatigue life of 2024 Al alloy, *Thin Solid Films* 515 (2006), pp. 1187–1191.

[18] E. Cirik and K. Genel, Effect of anodic oxidation on fatigue performance of 7075-T6 alloy, *Surf Coat Technol* 202 (2008), pp. 5190–5201.

[19] S. Ishihara, Z.Y. Nan, A.J. McEvily, T. Goshima and S. Sunada, On the initiation and growth behavior of corrosion pits during corrosion fatigue process of industrial pure aluminum, *Int J Fatigue* 30 (2008), pp. 659–1668.

[20] Z. Y. Nan, S. Ishihara and T. Goshima, Corrosion fatigue behavior of extruded magnesium alloy AZ31 in sodium chloride solution, *International Journal of Fatigue*, Vol. 30, No. 7, pp.1181-1188, 2008.

[21] M. Nishida, Stress concentration, Morikita Publishing Co., Ltd., Tokyo (1967) p. 526–529.

[22] A.J. McEvily, A method for the analysis of the growth of short fatigue cracks. In: J. Pokluda, Editor, *Materials structure and micromechanics of fracture*, Trans Tech Publications, Switzerland (2005) p. 3–10.

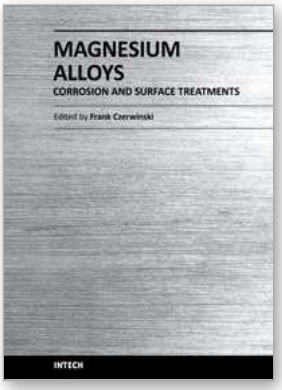

Magnesium Alloys - Corrosion and Surface Treatments
Edited by Frank Czerwinski

ISBN 978-953-307-972-1
Hard cover, 344 pages
Publisher InTech
Published online 14, January, 2011
Published in print edition January, 2011

A resistance of magnesium alloys to surface degradation is paramount for their applications in automotive, aerospace, consumer electronics and general-purpose markets. An emphasis of this book is on oxidation, corrosion and surface modifications, designed to enhance the alloy surface stability. It covers a nature of oxides grown at elevated temperatures and oxidation characteristics of selected alloys along with elements of general and electrochemical corrosion. Medical applications are considered that explore bio-compatibility of magnesium alloys. Also techniques of surface modifications, designed to improve not only corrosion resistance but also corrosion fatigue, wear and other behaviors, are described. The book represents a valuable resource for scientists and engineers from academia and industry.

INTECH
open science | open minds

InTech Europe
University Campus STeP Ri
Slavka Krautzeka 83/A
51000 Rijeka, Croatia
Phone: +385 (51) 770 447
Fax: +385 (51) 686 166
www.intechopen.com

InTech China
Unit 405, Office Block, Hotel Equatorial Shanghai
No.65, Yan An Road (West), Shanghai, 200040, China
中国上海市延安西路65号上海国际贵都大饭店办公楼405单元
Phone: +86-21-62489820
Fax: +86-21-62489821